5

Resonant metagratings for spectral and angular control of light for colored rooftop photovoltaics

Open your eyes, look up to the skies and see

Bohemian Rhapsody – Queen

We design semi-transparent metagrating supercells that enable control over the spectrum and directivity of incident light for applications in photovoltaics with tailored angular appearance. The building block of the supercells is a 110-120 nm wide and 175 nm tall silicon nanowire that shows a strong Mie resonances around λ = 650 nm. By arranging the resonant Mie scatterers into metagratings of increasing pitch (675-1300 nm) we create a Lambertian-like scattering distribution over an angular range of choice. The millimeter-sized metasurfaces were fabricated using electron beam lithography and reactive ion etching. The fabricated metasurface nearly fully suppresses specular reflection on resonance while 10% of the incoming light around the resonance is scattered into the angular range between 30-75°, creating a bright red appearance over this specific range of angles. Off-resonant light in the blue, green and near-infrared is efficiently transmitted through the metasurface and absorbed in the underlying photovoltaic cell. The implemented silicon heterojunction solar cells with integrated metagrating supercells show a reduction in external quantum efficiency matching the resonant scattering spectral range. The short circuit current is reduced by 13% due to the combined effects of resonant scattering, reflection from the high-index substrate and absorption in the Si nanowires. In addition, to efficient colorful photovoltaics with tailored angular appearance, the metagrating concept can find application in many other light management designs for photovoltaics and other opto-electronic devices.

5.1. Introduction

New solar power conversion architectures are increasingly important to achieve large-scale sustainable power generation to sustain the growing energy needs of our society. Integration of photovoltaics (PV) into the local architecture, buildings and urban terrains is a rapidly growing research and technology area and will be crucial to meet the requirements set by the Paris agreement in the coming years [81]. Current commercial solar cells and modules typically have a blue or black color that does not always fit within the urban design. Modules with tailored color are necessary to integrate PV into residential and modern city building architecture, where aesthetics plays a key role. In order to achieve both functional beauty and high power conversion efficiency, it is essential to develop innovative PV solutions to create colored solar cells while maintaining high efficiencies.

Over the last decades, research has shown different approaches to achieve colored PV. Interference coatings and Bragg reflectors have been used to modify the reflected spectrum, but do not offer control over the angular scattering [18, 19, 21, 82, 83]. Colored optical coatings, based on polymer or luminescent materials have been applied on the front module glass of cells [84–87], but are often limited by absorption in the coating material. Other solutions, specifically for solar roof tiles, have been offered to control the field of view with louver films that shade the cells on a rooftop for observers from the ground [88]. This simple approach shows esthetical results; however, the performance of the solar cell is highly restricted if the sun shines at a low angle, because the louver film also shades the sunlight. Scattering from plasmonic nanostructures has been applied in colorful solar cells, but suffers from fundamental optical losses in the metal [27, 89]. Similarly, resonant dielectric nanoparticles have been used for spectrally controlled light scattering with minimal optical losses [43–47]. Recently, these nanostructures have been employed for the creation of colorful solar cells, with the advantage of very little losses and scalable fabrication possibilities [24, 25, 90].

So far, none of the proposed designs for colored PV exhibits both angular and spectral control on the reflected light. The possibility of designing the scattering angular profile at will is particularly appealing in colored PV applications for two main reasons: first, for a colored surface to appear matte its angular reflectance has to follow the Lambertian cosine law (i.e., the apparent brightness of the scattered light should be the same for an observer from every angle). Second, it is important to reflect the color to a specific field of view of choice in order to minimize the losses as much as possible. The most obvious example is the application of directional colored solar cells on rooftops, where a red color appearance should be seen only from an observer near the building, while reflection upwards is undesired.

The use of scattering dielectric nanoparticles allows controlling not only the spectrum, by exciting Mie resonances, but also the directivity by smartly arranging the scatterers into a metasurface. In previous studies, different metasurfaces, specifically metagratings, have been introduced to allow directional control of resonant reflection [71, 72, 74–78, 91]. In this work we demonstrate how the geometry of an array of dielectric Mie-scatterers arranged in a grating structure can be tailored such that light in a narrow spectral band is scattered over a well-defined angular range. To this end, we design a supercell of multiple metagratings consisting of dielectric nanoparticles that shows

Lambertian resonant scattering while the non-resonant spectral bands are effectively transmitted. We demonstrate these concepts in a one-dimensional geometry employing Mie resonances in subwavelength silicon nanowires (NWs) that allow us to gain spectral control over the reflected light for one polarization direction; the design can be readily expanded to two dimensions. The scattering resonances are tuned by optimizing the shape and spatial dimensions of the nanowires such that the scattering profile matches the desired scattering spectrum. We demonstrate resonant scattering around λ = 650 nm, yielding a red scattering profile. Next, the NWs are placed in multiple gratings on a transparent substrate that scatter light with a tailored distribution over the first diffraction orders. We apply the metasurface onto a Si solar cell and demonstrate that effective light scattering in a narrow spectral and angular band is combined with high external quantum efficiency of the solar cell.

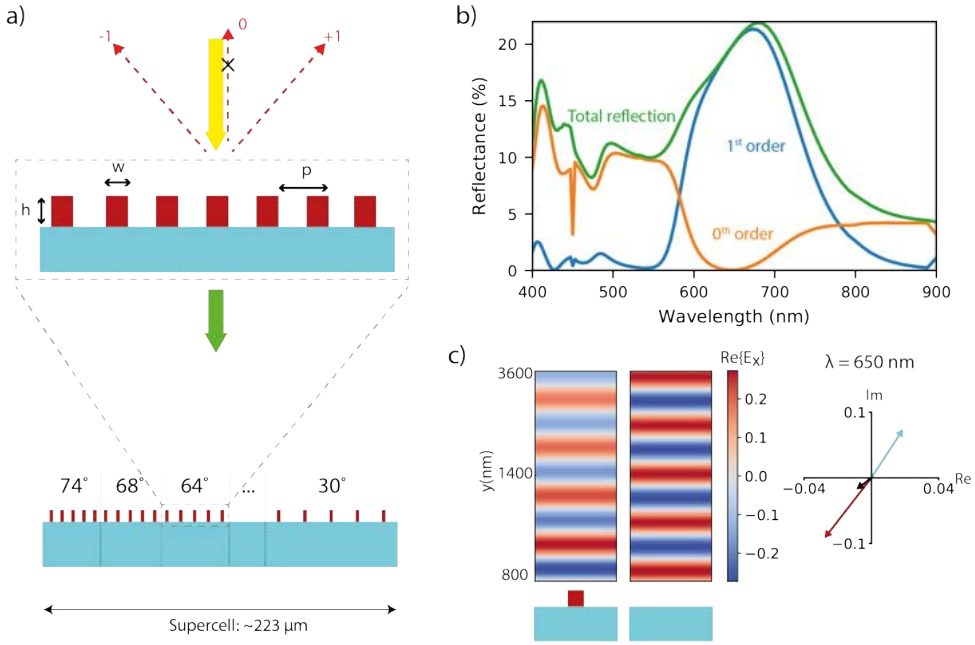

Figure 5.1: Principle of transparent metagrating. a) Top: Schematic overview of a transparent metagrating. Mie silicon nanowire resonators are placed periodically on top of a transparent substrate. The light around the resonance is scattered into diffraction orders. Bottom: Schematic overview of the complete supercell design. 25 metagratings are placed next to each other to form a supercell that reflects light around the resonance wavelength towards an angle range of 30°-75° b) Simulated reflectance of a metagrating of silicon resonators (w = 110 nm, h = 175 nm, p = 900 nm). The total reflectance (green line), specular reflectance (orange line) and diffraction into the first (+1 and -1) order (blue line) are plotted. c) Scattered E field radiated upwards from the single nanowire (left) and field reflected off the sapphire substrate (right) at the wavelength of cancellation λ = 650 nm. Phasor representation of the scattered E field from the nanowire array (red arrow) and the substrate (light blue arrow), and their sum (black arrow).

5.2. Theory and design

In this section, we introduce the concept of a Mie-resonant metagrating and outline how to leverage its properties to tailor at will the spectral and angular response of the metasurface. Specifically, for rooftop PV applications, we design the response to correspond to a Lambertian angular profile spectrally peaked in the red portion of the visible spectrum. Different from previous approaches [91], the Mie-resonators are placed on a transparent substrate such that only the resonant portion of the spectrum is reflected, while the transmitted light can be conveniently collected by a solar cell (see Figure 5.1). Upon excitation of Mie resonances, high-index dielectric nano-antennas can strongly scatter the incoming light [41, 44, 51]. In particular, here we exploit the modes sustained by NWs made of silicon, taking advantage of its high refractive index. The scattering unit cells of the metasurface are composed of Si NWs of height h = 175 nm and width between w = 100-120 nm on a sapphire substrate. The resonant wavelength of modes supported by such a high index scatterer can easily be tuned by changing the size of the scatterer, thus enabling spectral control. Details about the scattering cross section of the single Si NW are given in the SI. In this work the metasurface is designed to scatter light within a narrow bandwidth around λ = 650 nm.

Next, the Mie scatterers are placed into an array with periodicity p, such that first-order diffraction in air occurs while the second order is still evanescent. This is the case for periodicities in the range 650 nm < p < 1300 nm, according to the grating equation for normally incident light $p\sin(\theta_m) = m\lambda$, where θ_m is the angle at which light is diffracted, m is an integer denoting the order of diffraction and λ is the wavelength of the incident light. In this work, as light is normally incident on the grating, two symmetric 1^{st} (+1 and -1) diffraction orders exist that we refer to as 1^{st} orders from now on. Figure 5.1b shows the simulated [92, 93] reflectance spectrum of a single grating with pitch p = 900 nm, where the unit cell is composed of a single Si NW (w = 110 nm, h = 175 nm) on sapphire and it is illuminated at normal incidence by a plane wave polarized perpendicular to the NW (TE polarized). The reflectance into the 0^{th} and the $\pm1^{st}$ diffraction orders (θ_1=±46.2° at λ = 650 nm) reveals three important features. First, a clear peak around the design resonance λ = 650 nm (~20%) is observed due to resonant excitation of the modes of the Si NWs around this wavelength. Second, another peak around λ = 410 nm is observed (~15%), originating from a higher-order mode excitation. Third, a significant portion of the green and blue spectral range is directly reflected off the sapphire substrate to the 0^{th} order (~10%). It is important to note that most of the reflected light around the resonance is scattered into the 1^{st} orders (20%), while reflection back to the 0^{th} order is suppressed (~2%).

In order to investigate the physical mechanism behind the suppression of specular reflection we use the Total Field Scattered Field method [94]. In fact, light resonantly scattered by the NWs is interfering destructivelylight reflected off the bare sapphire substrate, hence resulting in a suppressed reflection to the 0^{th} order. In detail, for destructive interference to appear the amplitude of the scatteredreflected light from the substrate and theat scattered by the NWs is designed to be equal, while the phase is shifted by π. This cancellation phenomenon is expounded in Figure 5.1c by investigating the scattered fields of the two scenarios. The field scattered by a single NW (left) and that reflected by the sapphire substrate (right) is shown, when illuminated at normal inci-

dence by a plane wave at λ = 650 nm (TE). In the first case, the total field scattered filed approach allows to only look at the scattering contribution of the NW, and not of the substrate. Importantly, only the upward scattering in specular direction is shown here. The outgoing specular reflected field from the bare sapphire substrate shows a clear phase shift compared to the scattered field of the NW. In addition, the phasor representation at a position in the backward scattering direction of the scattered (NWs) and reflected (bare sapphire) fields is shown for λ= 650 nm. In the complex plane the electric field of the scattered light is depicted for both scenarios and allows precise comparison of the amplitude (length of arrow) and phase (angle in complex plane). In detail, for the NW scenario the amplitude was taken from the scattered wavefront of an array of NWs (pitch p = 900 nm), as the amplitude of a single NW is decreasing radially. The phase of the scattered field in backward direction is equal for a single NW or a NW array. Notably, it can be seen that the phase shift is almost π while the amplitude is close to equal at the wavelength of cancellation. The sum of the two vectors (black vector) shows that the cancellation is close to ideal. The reflection from the substrate is thus fundamental to achieve the cancellation in specular direction as discussed in more detail in the Supporting Info (5.4) and also explained in [91].

By considering different pitches, each targeting a different outgoing angle of diffraction, and suitably combining them into a larger supercell, it is possible to design a prescribed overall angular response. A schematic overview of the design, resulting in a supercell that scatters from 30-75° for λ = 650 nm (pitch: 675 – 1300 nm), is presented in the bottom of Figure 5.1a.

In colored PV applications, it is important that a Lambertian reflected angular profile is achieved to perceive a matte appearance [25]. However, in rooftop PV applications this requirement can be relaxed since the metasurface should appear Lambertian red only from an observer on the street. Hence, assuming that the sun is incident normal to the solar cells on a rooftop, we can disregard small diffracted angles in the design. Since common house roofs have an angle of ~40°, the desired angular span of the designed angular response lies in the range 30-75°. Indeed, sunlight that hits the panel perpendicular is scattered towards the field of view of pedestrians on the street. Ideally, the scattering should happen asymmetrically only towards the ground, not towards the sky. This could be realized by employing asymmetric scattering unit cells [76, 95], but has not been center of research in this work. As mentioned before, the overall structure is realized by placing multiple metagratings next to each other, creating a "supercell" array of silicon nanowires with varying periodicities (see Figure 5.1a). Within this procedure, it is also important to take into account the relative area of each metagrating (adjusted by their own efficiencies) in order to properly reproduce the Lambertian intensity distribution in reflection. The total area of the supercell is the sum of all grating areas, and adds up to 223 µm. The specific values of p, w, the total reflection and reflection to the 1^{st} order for individual metagratings and the number of unit cells used in each of the metagratings composing the supercell are summarized in Table 5.1.

5.3. Experiments

In order to experimentally demonstrate the possibility of gaining angular and spectral control via transparent metagratings we fabricated the structure described above and

characterized it optically. Next, we compare the measured data to numerical simulations, and assess the performance of a solar cell with the optimized metasurface integrated into its structure.

5.3.1. Fabrication

The metagratings were fabricated using Electron Beam Lithography (EBL), as described in the following. First, silicon-on-sapphire substrates (500 nm c-Si on 0.46 mm R-plane sapphire, MTI Corporation) were cleaned in base piranha. The silicon layer is etched down to a thickness of 175 nm using Reactive Ion Etching (RIE) using a CHF_3 (15 sccm) - SF_6 (10 sccm) - O_2 (3 sccm) plasma etch. Next, a 50-60 nm HSQ high-resolution negative resist layer was spin-coated on the sample, and baked for 150 seconds at 180 °C. For better conductivity, Electra 92 (AR-PC-5091) was spin-coated on the sample. The substrate was then exposed using a Raith Voyager lithography system (dose of 2.400 μC/cm^2). To obtain a sample that is large enough for optical measurements, the supercell of 223 μm described above is replicated 6 times next to each other, resulting in a 1.35 mm wide field. After e-beam writing, the sample was developed in TMAH for 75 seconds at 50°C. The patterned HSQ is then used as a hard mask to structure the underlying Si layer using two subsequent RIE etching steps. First, the native oxide of the silicon is etched using Cl_2 (60 sccm), then the silicon is etched in a HBr (48.6 sccm) and O_2 (1.4 sccm) plasma at 60°C.

The result of the described fabrication is shown in Figure 5.2. The sample consists of silicon NWs with a remaining HSQ layer on top, on a sapphire substrate. A single NW is depicted in Figure 5.2a and b, showing that the side walls are etched perpendicular to the substrate. The HSQ on top of the nanowire is not removed as this process involves chemical reactions that also react with the sapphire substrate. For better resolution, a layer of Electra 92 (AR-PC-5091) was spin-coated on the sample before imaging. An overview SEM image of the total supercell is shown in Figure 5.2c. The pitch between the wires is decreasing from left (p = 1300 nm) to right (p = 675 nm) and for the complete area of the supercell a good uniformity was achieved. On the right side of the supercell, the beginning of the next identical supercell is visible.

5.3.2. Optical characterization

To distinguish light reflected specularly (0^{th} order) from light reflected at an angle (1^{st} orders), we use an integrating sphere. We measure both the sample's total reflectance and the total reflectance excluding the 0^{th} order. The difference between the two measurements then yields the 0^{th}-order reflection (see Supporting Info (5.4) for a schematic of the setup).

Figure 5.3a shows the measured specular reflectance spectrum, as well as the total reflectance spectrum excluding the specular contribution, which we refer to as scattered spectrum. The latter shows a broad peak centered at of λ = 614 nm reaching 9.9% reflectance. The full width at half-maximum of this peak is around 200 nm, covering the wavelength range of interest for red color perception. At the same time, in the same bandwidth around λ = 614 nm, the 0^{th}-order reflection is strongly suppressed, as desired. Indeed, the 0^{th}-order reflectance is around 8% in the blue wavelength range and decreases to 2% on resonance demonstrating efficient light redirection. Additionally, the

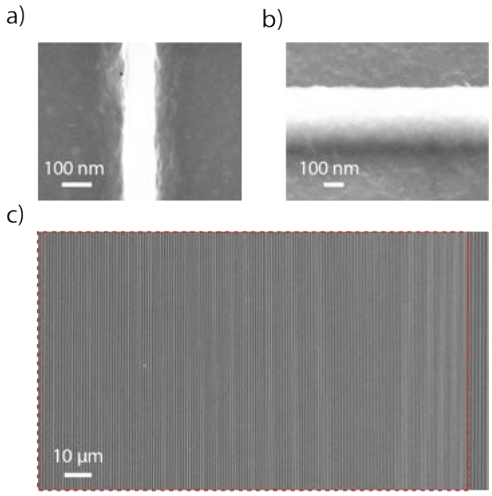

Figure 5.2: SEM image of fabricated metasurface. a) Top-view SEM of a single silicon nanowire of w = 120 nm on top of sapphire substrate b) Tilted image of a single silicon nanowire (tilt angle 45°) c) Top-view of full supercell (dashed red line) containing all metagratings with varying pitch (p = 675 nm – p = 1300 nm). Stitching of two supercells can be seen on the right side of the image.

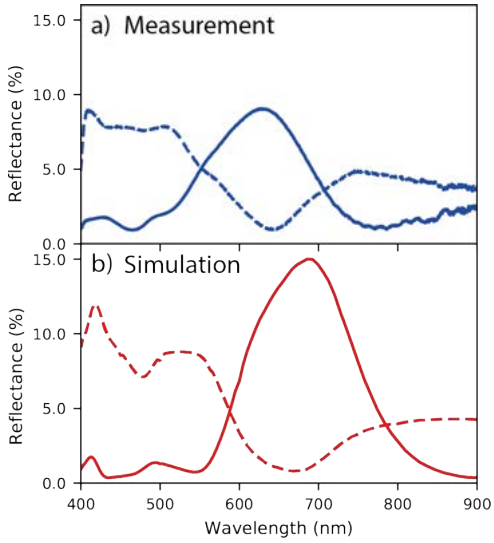

Figure 5.3: Reflectance spectra of full metasurface. a) Measured specular reflectance spectrum (dashed blue line) and scattered spectrum (solid blue line) of full metasurface. b) Simulated specular reflectance (dashed red line) and reflectance for diffraction order (solid red line) of a single supercell. Reflectance is determined by the contribution of the different metagratings in the supercell, weighted by their area respectively.

reflection at wavelengths above the resonance is slightly decreased.

Figure 5.3b shows simulated scattered and specular reflectance spectra. The exper-

imentally measured trends show good agreement with the simulated spectra: a broad peak around 680 nm in the averaged 1^{st} order reflection (average reflectance to 1^{st}–orders: sum of the reflectance from the different metagratings composing the metasurface, weighted by their relative area) corresponds to a clear reduction in specular reflection. The position of the peak can be explained by the combined contributions of the different metagratings (see section 5.4). We ascribe the lower measured reflectance compared to the simulations to fabrication imperfections resulting in silicon NWs with slightly different dimensions, as well as small slanting of the sidewalls which results in a less pronounced resonance [96].

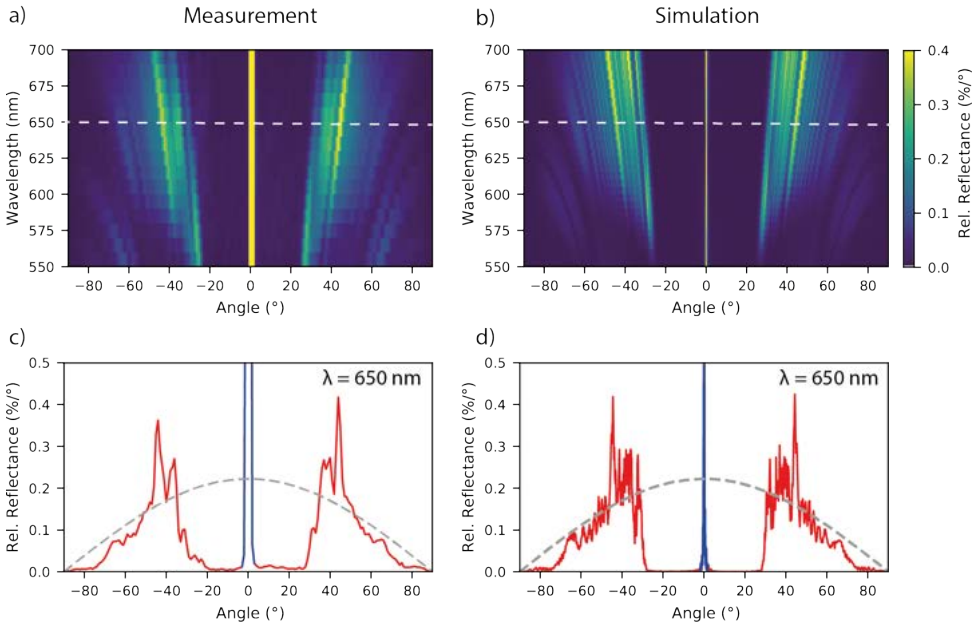

Figure 5.4: Angle-resolved reflectance. a) Measured and b) simulated angular reflectance of full metasurface. White dashed lines indicate cross section of the reflectance shown in c) and d). c) Angular reflectance at λ = 650 nm with specular (blue solid line) and diffracted (red solid line) contributions. The scattering profile of a perfect Lambertian scatterer is plotted as well (gray dashed line). d) Simulated data as in c).

Figure 5.4a shows the angular reflectance as a function of wavelength, measured using a rotating stage setup (see [91] for the description of measurement setup). The measurements were performed in the wavelength range λ = 550-700 nm in steps of 10 nm. First of all, as designed, the sample does not scatter light to angles below 30° and above 75°. As mentioned earlier, the design is optimized to have only the 1^{st} diffraction orders at $\lambda \geq 650$ nm. This can be observed in the measured spectra (Figure 5.4a). For shorter wavelengths $\lambda \leq 650$ nm, 2^{nd}-order diffraction in reflection is noticeable at high angles. Furthermore, following the grating equation, the diffraction angle for each metagrating increases as the illumination wavelength increases. The measurement significantly reflects very similar features in the simulated angular reflectance spectra in Figure 5.4b.

Figure 5.4c shows the measured angular reflectance at λ = 650 nm. The scattered

part of the light is depicted in red, whereas the grey dashed line represents the ideal Lambertian cosine distribution. Experimentally, the angular reflectance follows the desired cosine law rather well for angles in the range 30-75°. The two high reflection peaks at 45° are the result of a non-ideal design ; they are also visible in simulations (see Figure 5.4d and Table 5.1). The blue part of the angular reflectance represents the 0^{th}-order reflection and peaks at 6.8 %/° and 3.0 %/° in experiment and simulations, respectively (out of scale in Figure 5.4c and d). We observe a broader reflection range for the 0^{th} order peak in the measurement compared to that in simulation, due to a difference in binning (0.18° in simulation versus 1.0° in measurement). Overall, we conclude that the experimental results follow the simulation results with a good agreement.

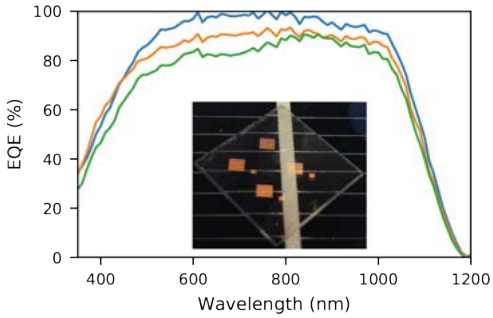

Figure 5.5: External quantum efficiency measurements. Measured external quantum efficiency of bare silicon heterojunction cell (blue line), with bare sapphire on top (orange line) and with metasurface (green line). Inset: Photograph (taken under 45°) of the sample attached to the silicon solar cell using immersion oil. The sample size is 12×12 mm. The four red patches are four metasurfaces with the same underlying design, but fabricated with a slightly different dose during e-beam lithography. On the solar cell silver contact fingers (horizontal grey lines) and a busbar (vertical grey line) can be seen.

5.3.3. Electrical characterization

Next, we apply the transparent metagrating on a Si solar cell. The nanopatterned sapphire substrate was placed on top of a heterojunction silicon solar cell using immersion oil (Fluka 10976, n=1.52) (same setup as in [24]). The cell features a textured front surface and a standard anti-reflection coating. We measured the External Quantum Efficiency (EQE) for three different cases: bare solar cell, cell with clean sapphire substrate and cell with the fabricated metagrating sample (see Figure 5.5). With the sapphire substrate in place, we observe a similar trend as for the bare silicon solar cell, with slightly lower EQE over the whole spectrum. The reduction in EQE is due to reflection of light from the front surface of the sapphire, which is around 8% over the visible wavelength range. The EQE of the cell with the metagrating sample on top is lower compared to the EQE of the cell with sapphire, especially below λ = 800 nm. A closer inspection of the spectrum, shows a reduction of the EQE from λ = 600-800 nm, which is due to the as-designed enhanced reflection shown in Figure 5.3a. The inset in Figure 5.5 shows a photo taken under 45° of the sample placed on top of the solar cell. The bright red rooftop-like colored reflection is clearly visible. In the lower wavelength range, the EQE is reduced due to the higher absorption in the silicon nanowires. This could potentially be reduced by replacing the

silicon with a material with a lower absorption in the visible range (e.g. TiO_2). The measured short circuit current density for the bare silicon solar cell is J_{sc} = 38.9 mA/cm^2. Including the metagrating sample on top slightly reduces the value to J_{sc} = 34.0 mA/cm^2. This implies that to first order the cell efficiency is reduced by relative 13% due to the narrow-angle colored scattering metasurface.

5.3.4. Conclusion

In this work, we experimentally demonstrated spectral and angular control of scattered light using resonant metagratings for colored photovoltaics. Silicon nanowires were fabricated on a transparent substrate and resonantly scatter light around λ = 650 nm. The nanowires were placed in a supercell structure composed of multiple gratings with different pitches, creating a Lambertian scattering distribution with specular reflection nearly fully suppressed and efficient transmission outside the resonant scattering band. The supercell structure was designed to backscatter light within the 30-75° range and experiments and simulations are in very good agreement. The metagratings are integrated with a silicon heterojunction solar cell creating a bright red scattering appearance under a limited range of angles, as desired, and enable seamless integration with roof tile geometries. The external quantum efficiency is only reduced in the scattering spectral band, with a short circuit current drop of only 13%. Potentially, future asymmetric designs can further enhance the efficiency by scattering light only to the ground and not to the sky. The nanopatterned geometries can be readily fabricated and upscaled to practical PV applications with some reinvestment in materials and methods. In particular, the materials used in this work could easily be replaced by more practical materials- For example, the module glass could serve directly as the transparent substrate and any dielectric high index material (polymer, amorphous Si, etc.) for the scatterers. Large-scale fabrication techniques might need further investigation, but promising routes such as spray-coating and substrate conformal imprinting lithography [38] could replace the lab-scale methods.

5.4. Supplementary

5.4.1. Scattering of Mie resonator

Figure 5.6 shows the simulated [92, 93] normalized scattering cross section (optical scattering cross section normalized by the geometrical cross section) for a Si NW of height h = 175 nm and width w = 110 nm on a sapphire substrate, illuminated at normal incidence by a plane wave polarized perpendicularly to the axes of the NW (TE polarization). The peak around λ = 720 nm marks the excitation of the magnetic dipole mode (MD), while higher order modes appear at shorter wavelengths. The inset of Figure 5.6 shows the H field intensity profile at the MD resonance. The resonant wavelength of such modes can be easily tuned by changing the size of the scatterer, thus enabling the required spectral control. Comparing the scattering cross section with the spectrum of reflectance in Figure 5.1b in the main text, raises the question why the reflectance peak is located at 650 nm for the scatterer in a periodic metagrating. The angular radiation pattern of the modes of the single scatterer determines the scattering towards different directions.

However, light can only be scattered to the accessible channels (reflection, transmis-

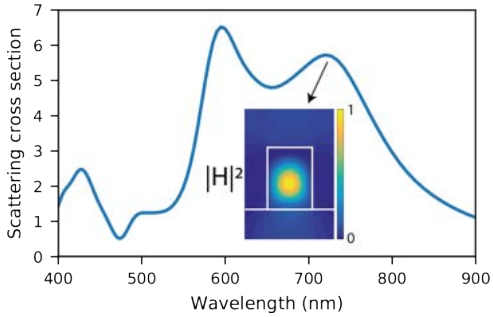

Figure 5.6: Simulated normalized scattering cross section of a single silicon nanowire (w = 110 nm, h = 175 nm) on top of a sapphire substrate. The inset shows the magnetic field intensity profile at the magnetic dipole resonance at 720 nm.

sion, diffraction). The spectrum to those fixed pathways is thus given by the radiation pattern. But there are other effects that have to be taken into account. In the case of this work, the reflection from the substrate cancels the 0 order reflection pathway and the light is thus funneled to the diffraction orders or to transmission, even though the radiation pattern might as well radiate upwards. Also, if the scatterers are getting closer their might be coupling between the particles and new modes appear that can influence the radiation direction. The exact analysis of the modes and their radiation patterns and interaction is beyond the scope of this work. To this end, a particle with resonances in the wavelength range of interest (λ = 630 nm – 670 nm) was taken as a starting point and optimized as unit cell in a metagrating to achieve high diffraction to the 1^{st} order and as such cancellation of the 0^{th} order.

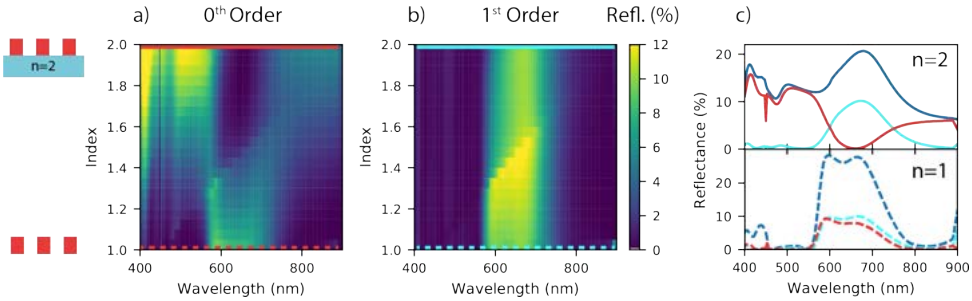

Figure 5.7: Simulated reflectance of a metagrating of silicon resonators (w = 110 nm, h = 175 nm, p = 900 nm) with changing substrate index (n=1-2). Front inset: Schematic of metagrating on a substrate or without substrate. a) Specular reflectance (0^{th} order) and b) diffraction into 1^{st} order. The cyan and red lines indicate the crosscuts of specular reflectance and diffraction plotted in c) respectively. Reflectance above 12% is saturated for better visibility. c) Bottom: The total reflectance (blue line), specular reflectance (cyan line) and diffraction into the first order (red line) of a metagrating without a substrate (n=1); Top: Same as bottom graph, with metagrating on substrate with index n=2.

5.4.2. Metagrating efficiency

As highlighted in the main text, our metagrating design efficiently steers light into the 1^{st} diffraction order by canceling the specular reflection (0^{th} order). This is due to the destructive interference between light directly reflected off the substrate and light that is resonantly scattered by the nanowires. In Figure 5.7, this effect is illustrated by plotting the simulated reflectance of a metagrating while varying the index of the substrate from n=1 to n=2. This in turn modifies the relative contribution between the scattered light and the light reflected non-resonantly from the sapphire substrate. The latter contribution is zero when n=1.

The simulated metagrating is the same as in Fig. 5.1c in the main text (width = 110 nm, height = 175 nm, pitch = 900 nm). As the substrate's index is increased, the relative specular reflectance to the 0^{th} order shows a decrease (Fig. 5.7a) while the diffraction to the 1^{st} order increases (Fig. 5.7b) for an illumination wavelength close to the resonance (λ = 650 nm).

In fact, without the substrate the nanowires scatter isotropically, while introducing a substrate and increasing its index, the specular reflection is suppressed and the diffraction efficiency increases. To corroborate this, we plot the extreme cases of a low and a high substrate index in Fig. 5.7c. With no substrate in place (Fig. 5.7c – lower panel), the reflectance to the 0^{th} order is equal to the scattering towards the 1^{st} order (isotropic scattering). On the other hand, for a substrate with index n=2 (Fig. 5.7c – upper panel), the 0^{th} order reflectance is completely suppressed. In the case of our experiment the substrate is sapphire (index = 1.7) and the 0^{th} order reflection can almost be canceled completely.

5.4.3. Parameter overview

The specific parameters of the metagratings composing the supercell are summarized in Table 5.1

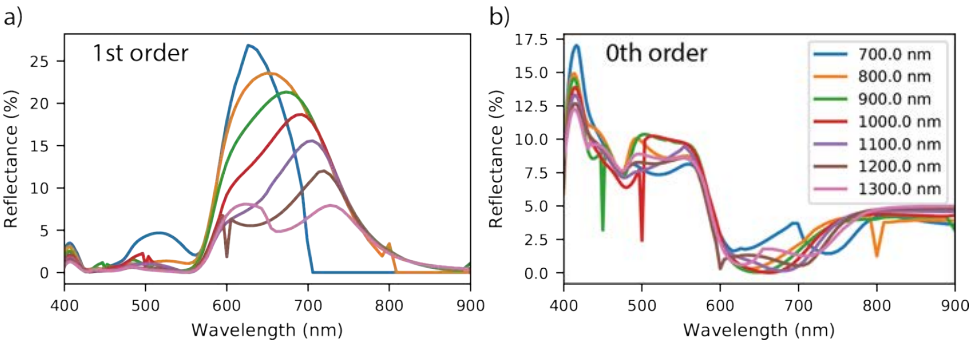

Figure 5.8: Simulated reflectance of metagratings of silicon resonators on a sapphire substrate (w = 110 nm, h = 175 nm, p = 700 nm – 1300 nm) into 1^{st} order and 0^{th} order

pitch [nm]	width [nm]	number of particles	angle [degree]
675	120	6	74
700	120	7	68
725	120	7	64
750	120	7	60
775	120	7	57
800	120	7	54
825	120	8	52
850	120	8	50
875	120	8	48
900	120	9	46
925	120	9	45
925*	120	9	45
950	120	9	43
975	120	9	42
1000	110	10	41
1025	110	9	39
1050	110	10	38
1075	110	10	37
1100	110	10	36
1125	110	10	35
1150	100	10	34
1200	100	11	33
1225	100	11	32
1250	100	11	31
1300	100	12	30

Table 5.1: Overview of design parameters of all metagratings. *The metagrating with a pitch of 925 nm was accidently put twice in the design/fabrication.

5.4.4. Reflectance with changing pitch

The metasurface is composed of metagratings with changing pitch in order to create a large range of diffraction angles as explained in the main text. Every individual metagrating was optimized to highest diffraction in a bandwidth of λ = 630 nm – 670 nm. Metagratings with NWs of the same dimensions (w = 110 nm, h = 175 nm) on a sapphire substrate with a changing pitch (p = 700 nm – 1300 nm) are simulated (Figure 5.8). In figure 5.8a the diffraction for different pitches is plotted. The strength of the reflectance is related to the strength of the scattering of the unit cell. Consequently, with increasing distance between the scatterers the overall reflectance is decreasing and so is the diffraction. In the supercell the peak of reflectance lies at 680 nm, which stems from the combined diffraction spectra of the different metagratings (See Figure 5.3). In the 0^{th} order reflectance it can be seen that the minimum does not change much between the different pitches. This is due to the fact that the cancellation process is mainly driven by the interference with reflectance of the substrate and does not change much between

different pitches.

5.4.5. Analysis of angle of incidence

The metasurface was optimized for normally incident light. As the position of the sun is changing along a day, it is important to study the operation of the metasurface with changing angle of incidence. In Figure 5.9a, the simulated angular reflectance of the full metasurface is shown with angles of incidence between 10 – 45°. For a wavelength of λ = 650 nm the angular scattering still follows the desired cosine distribution (grey dashed line), however, with a changed range of angles that depend on the change in diffraction orders. At higher angle of incidence, the metasurface supports as well 2^{nd} order diffraction at 650 nm that contribute to a wide range of reflected angles.

Next, the reflectance of a metagrating with a pitch of p = 900 nm, with the same angles of incidence as in Figure 5.9a between 10-45°. For small changes (around 10°) the resonant reflectance of the design is pretty stable. For higher incoming angles (20°) the resonance seems to disappear, but the cancellation process of the specular reflection is still efficient. For higher angles (30 and 45°), the reflectance peaks again around 700 nm, and specular reflection is still canceled. As mentioned earlier, the precise change of modes is out of the scope of this study. However, the arguments for the cancellation process still hold for different angles of incidence.

5.4.6. Integrating sphere measurement setup

We measured the scattering of the sample using an integrating sphere. There are two methods of measurements; either to measure the total reflection (Figure 5.10a; specular reflection plus all diffraction orders) or only the diffraction (Figure 5.10b; no specular reflection). For the first method, the conventional setup of the integrating sphere is used. The sample is tilted at the back of the sphere, such that all reflection is collected by the detector. In the second method the sample is placed perpendicular to the incoming light at the back of the integrating sphere. In the latter case, the specular reflected beam can escape from the front opening of the sphere, and only scattered and diffracted light is collected by the spectrometer. The specular reflectance shown in Figure 5.3a of the main text is determined by the subtraction of two measurements by the two different methods; the diffraction measurement is subtracted from the total reflectance. For the scattered spectrum in that same Figure the second method of the setup was used.

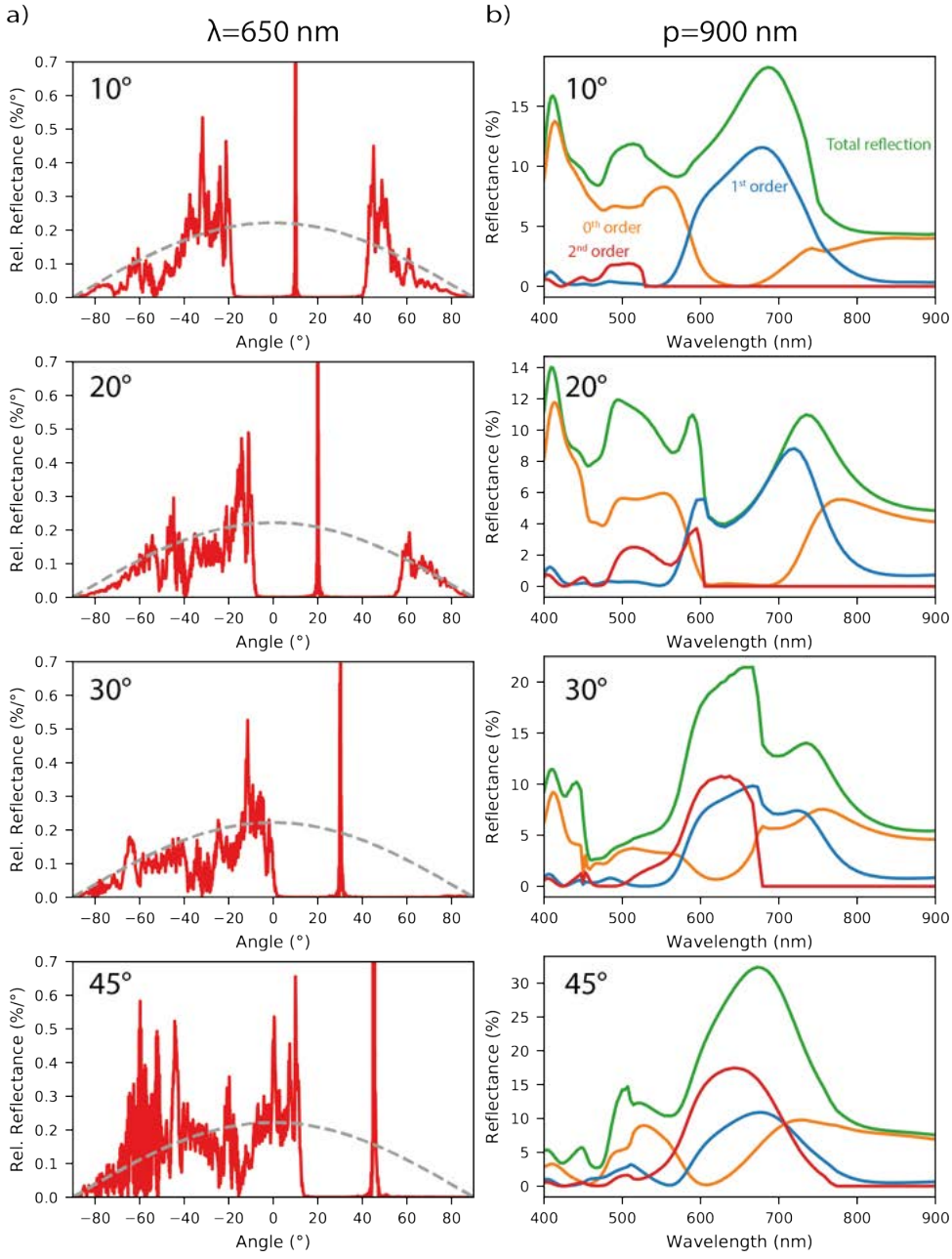

Figure 5.9: Analysis of changing angle of incidence a) Simulated angular reflectance at $\lambda = 650$ nm of full metasurface for angles from 10° - 45°. b) Simulated reflectance of metagrating as in Figure 5.1 c) with changing angle of incidence from 10° - 45°. The total reflectance (green line) is composed of specular reflectance (orange line), 1^{st} order diffraction (blue line) and 2^{nd} order diffraction (red line).

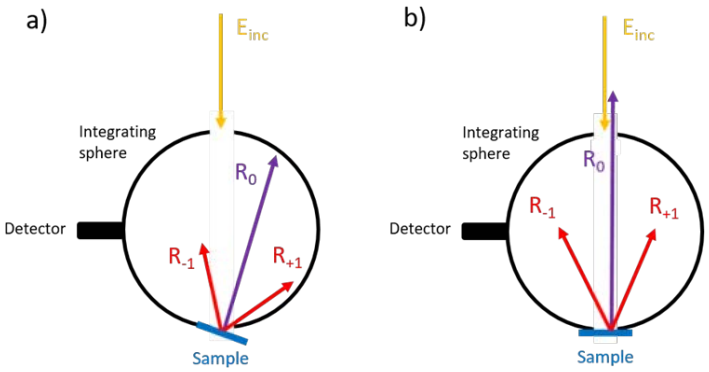

Figure 5.10: Integrating sphere setup a) Configuration with tilted sample; all scattered light is collected. b) Configuration with sample perpendicular to incoming light; specular reflection is not collected.